Materials Research Express

PAPER • **OPEN ACCESS**

X-ray diffraction profile analysis of green synthesized ZnO and TiO_2 nanoparticles

To cite this article: Penny Mathumba *et al* 2024 *Mater. Res. Express* **11** 075011

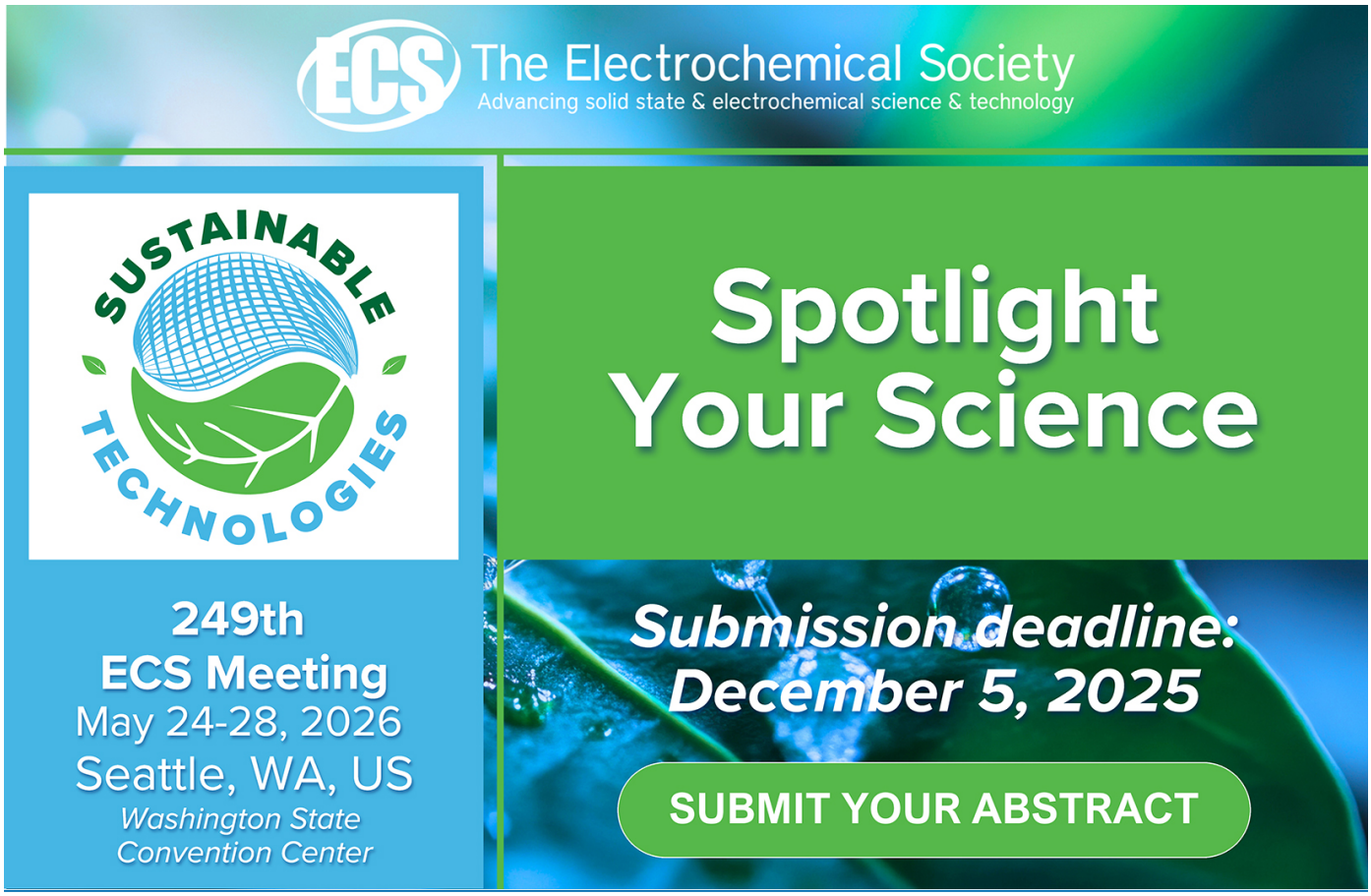

Materials Research Express

PAPER

X-ray diffraction profile analysis of green synthesized ZnO and TiO_2 nanoparticles

Penny Mathumba[1], **Mawethu P Bilibana**[2,3,*], **Olalekan C Olatunde**[2,3] and **Damian C Onwudiwe**[2,3]

[1] DSI/Mintek Nanotechnology Innovation Centre, Advanced Materials Division, Mintek, 200 Malibongwe Drive, Private Bag X3015, Johannesburg, Gauteng, South Africa
[2] Department of Chemistry, School of Physical and Chemical Sciences, Faculty of Natural and Agricultural Sciences, Mafikeng Campus, North-West University, Private Bag X2046, Mmabatho 2735, South Africa
[3] Material Science Innovation and Modelling (MaSIM) Research Focus Area, Faculty of Natural and Agricultural Sciences, Mafikeng Campus, North-West University, Private Bag X2046, Mmabatho 2735, South Africa
[*] Author to whom any correspondence should be addressed.

E-mail: Mawethu.Bilibana@nwu.ac.za

Keywords: plant-extract, hydrothermal, X-ray diffraction, william-hall, rietveld analysis, microstrain

OPEN ACCESS

RECEIVED
22 May 2024

REVISED
4 July 2024

ACCEPTED FOR PUBLICATION
16 July 2024

PUBLISHED
26 July 2024

Abstract

ZnO and TiO_2 nanoparticles were prepared through a plant-extract mediated hydrothermal synthesis. X-ray diffraction (XRD) study confirmed the crystalline nature and the phase characteristic of the obtained nanoparticles. X-ray diffraction profile analysis models such as Williamson–Hall analysis, size-strain plot and Rietveld analysis were further used in evaluating the microstructural parameters of the obtained materials. The calculated particle size for all the models was in great agreement, with values in the range of 55.46–87.6 nm recorded for ZnO, while for TiO_2, the crystallite size was in the range of 33.82–41.9 nm. The calculated crystal microstrain varied based on the model, while the stress in the ZnO and TiO_2 nanoparticles was evaluated at 3.8 and 13.7 MPa, respectively. Furthermore, TiO_2 nanoparticles had a higher energy density of 8.96×10^{-8} KJ m^{-3} compared to 7.12×10^{-8} KJ m^{-3} obtained for ZnO.

1. Introduction

Characterizing crystal structures is one of the most important tasks in the development of novel materials since it influences material properties [1]. X-ray diffraction is the main experimental technique used in exploring crystal information and x-ray diffraction peak profile analysis has emerged as a distinctive technique in exploring the microstructure of crystalline materials [2]. This technique is based on the broadening of x-ray diffraction peaks and it provides details about microstructural properties such as crystallite size, defects and lattice strains, which are important properties in material behavior [3, 4]. Since no crystal is perfect due to its finite size, the XRD peaks widen as a result of fluctuation from ideal crystalline material [5].

Lattice strain and crystal size are two primary causes of the XRD peaks broadening. The intrinsic crystal strain is typically caused by the large grain boundary area and the defective nature of crystalline materials. Although lattice dislocations are the primary cause of lattice strain, stacking faults, and triple-grain boundary can also have an effect. The size and inherent strain of the crystals have different effects on the Bragg peak, and the intensity of the peaks is influenced by the dominance of these effects [6].

The Scherrer method is a well-known method for calculating crystallite size using the XRD peak width, however, the technique does not take into account other factors that influence peak broadening such as the intrinsic strain and instrumental effect [7]. Therefore, other techniques which account for the strain in crystals such as the Averbach method, size-strain plot, and Williamson–Hall (W-H) method become very important in estimating the microstructural properties of crystalline materials. The W-H method is the simplest of all the techniques and also allows for the estimation of important elastic properties such as stress and strain [8, 9]. In the size-strain technique, the XRD peak profile is considered to be a combination of the Gaussian and Lorentz

functions [10]. This technique benefits from the less weight being given to the upper angle reflections, which usually give low precision [11, 12].

Biogenic synthesis is an easy technique for nanomaterial synthesis without the generation of toxic waste. They are therefore safe, eco-friendly and economical. Recently, various plant parts such as roots, fruits leaves and flowers have been explored for nanoparticle synthesis [13]. This technique avoids the use of expensive and toxic stabilizers, since biomolecules present in the plant extract act as both a reducing agent and stabilizing agent [14, 15]. ZnO and TiO_2 are two of the most studied semiconductor materials because of their unique optical and electronic properties. Furthermore, several studies have reported the green synthesis of these nanoparticles using various plant extracts [16–20]. The *Vachellia hebeclada* (*V. hebeclada*), also known as *Acacia hebeclada*, is a tree that is native to Southern Africa and has traditionally been utilized for therapeutic purposes [21]. To the best of our knowledge, the *V. hebaclada* plant has not been explored for the synthesis of metal oxide nanoparticles. Therefore, in this study, we report the synthesis of ZnO and TiO_2 nanoparticles, through a plant extract mediated hydrothermal process. Furthermore, the microstructural properties of the obtained nanomaterials were determined using different x-ray diffraction peak profile analysis models.

2. Materials and methods

All chemical reagents and solvents were purchased from Sigma-Aldrich (St Louis, Missouri, USA). and used as received without further purification. Ethanol absolute (99.5%), zinc nitrate hexahydrate reagent grade (98%), titanium tetraisopropoxide (TTIP, 99%), Sodium hydroxide (NaOH) pellets and sodium hydroxide (NaOH) were all obtained from Sigma-Aldrich (St Louis, Missouri, USA).

2.1. Extraction of phytochemicals from *V. hebeclada* for metal oxide synthesis

Cultivated *V. hebeclada* were collected from North-West University, Mololwana farm, Mafikeng, South Africa. These plants were grown per South African regulations using standard farming practices. Botanists from the North-West University authenticated their identities. The seeds were thoroughly washed under running water, dried at room temperature (24 °C), and powdered using a mortar. Pulverized seeds (500 g) were then boiled in (1.5 l) distilled water for 10 min before filtering, to obtain a dark brown powder. The extract was filtered and then concentrated under reduced pressure using a rotary evaporator at 70.1 °C. The dark brown powder obtained was dried under a high vacuum for an additional 16 h to constant mass.

2.2. Synthesis of ZnO and TiO_2 with *V. hebeclada seeds* extract powder

The metal oxide nanoparticles were synthesized via a facile hydrothermal approach using deionized water as a solvent. 5 g of *V. hebeclada* seeds extract powder was dissolved into 90 ml of water and magnetically stirred for 20 min until a homogenised solution was attained. Then 0.01 M zinc nitrate $(Zn(NO_3)_2.4H_2O$ was introduced drop by drop. The pH of the mixture was adjusted to 10 by adding 0.1 M NaOH solution. The mixture was autoclaved for 2 h at 121 °C 15 psi, resulting in the formation of bio-reduced precipitate at the bottom of the flask. After the reaction, the deposit was collected via vacuum filtration, and washed with deionized water and anhydrous ethanol two times, respectively. The resultant product was dried at 80 °C in a vacuum box overnight. Subsequently, the obtained precipitate was calcined in a furnace at 350 °C for 2 h to obtain ZnO nanoparticles. For the synthesis of the TiO_2 nanoparticle, 0.01 M of titanium tetraisopropyl (TTIP) was introduced into the plant extract solution and the procedure described for the ZnO nanoparticle was followed.

2.3. Characterization of ZnO and TiO_2 nanoparticles

The phases and crystallinity of the synthesized materials were identified using XRD and were carried out on a Bruker D8 Advance x-ray diffraction (Karlsruhe, Germany). The diffractometer has single wavelength Cu Kαradiation ($\lambda = 1.546060$ Å). The microstructural properties of the synthesized ZnO and TiO_2 nanoparticles such as crystallite size, lattice parameters and lattice strain were evaluated using the Scherrer equation, Williamson–Hall analysis, and Rietveld analysis. The Rietveld analysis was carried out using the X'Pert HighScore Plus software. The parameters refined include background, scale factor, lattice constants, profile half-width parameters (u, v, w) and isotropic thermal parameters. The pseudo-voigt model was used in modelling the peak profile function. The background was used without any correction factor [22].

3. Results and discussions

3.1. Microstructural properties of ZnO and TiO_2 nanoparticle

The XRD diffraction pattern of the green synthesized ZnO and TiO_2 nanoparticles (NPs) is shown in figure 1. The XRD pattern of TiO_2 NPs shows characteristic peaks that are indexed to the anatase phase of TiO_2, with

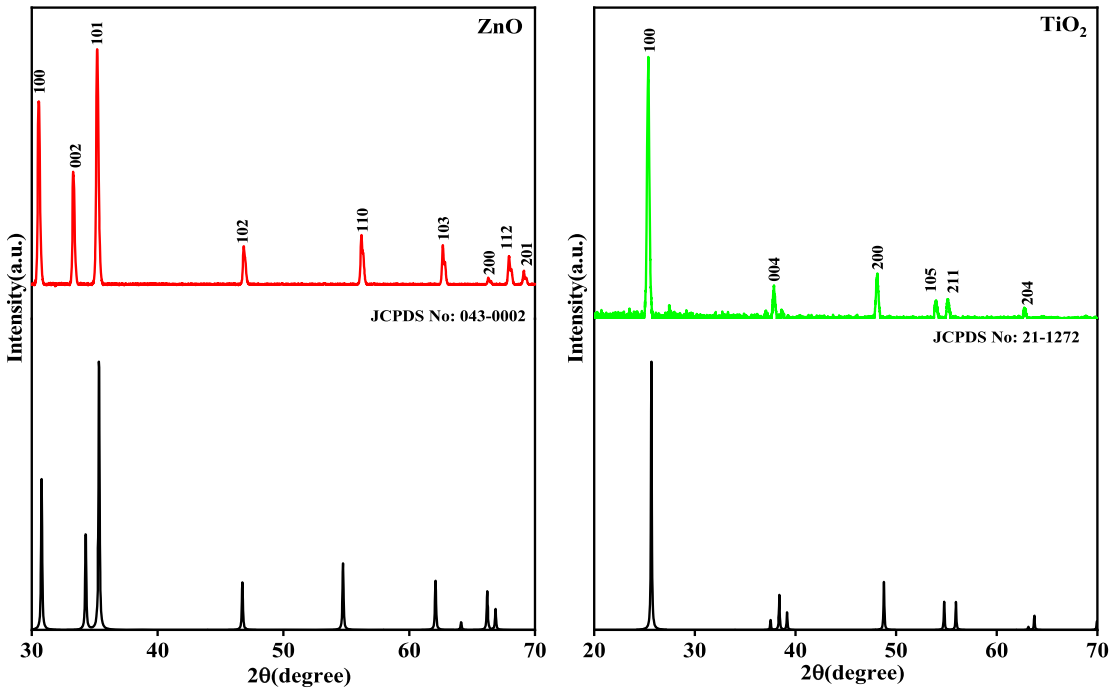

Figure 1. XRD pattern for (A) ZnO and (B) TiO_2 nanoparticle structural analysis.

tetragonal structure and space group 141 (JCPDS No. 21–1272) [23]. The diffraction pattern for ZnO showed well-defined diffraction peaks, which are in good agreement with the hexagonal wurtzite structure and space group P63mc (JCPDS No. 36–1451) [24]. The high intensity and sharpness of the XRD peaks of the nanoparticles showed the high crystallinity of the obtained nanoparticles [25].

The average crystallite size of the nanoparticles was calculated using the Scherrer's equation:

$$D = \frac{K\lambda}{\beta \cos\theta}, \tag{1}$$

where D is the average crystallite size (nm), K is the Scherrer constant (0.94), λ is the x-ray wavelength, (CuK_α = 1.5406 nm), β is the line broadening at FWHM in radians, and θ is the Bragg's angle in degrees [26]. The crystallite size of calcined ZnO nanoparticles was calculated to be 64.28 nm, while the crystallite size for TiO_2 was 34.47 nm. Particle size has been reported to play a significant role in the properties and application of nanomaterials [27]. The obtained crystallite size agrees with values reported in the literature for green-synthesized ZnO and TiO_2 [28, 29].

3.1.1. Williamson hall model

Scherrer's equation only takes into account how crystallite size affects peak broadening of XRD diffractions; strains in the lattice's microstructures, which can occur in nanocrystals as a result of stacking faults, grain boundaries, triple junctions, and point defects, are not taken into account [30]. By analysing the peak width as a function of 2θ, the Williamson–Hall analysis deconvolutes size and strain-induced broadening through a simplified integral breadth analysis [31]. The overall x-ray diffraction peak broadening could be written as:

$$\beta_{\text{total}} = \beta_{\text{size}} + \beta_{\text{strain}} \tag{2}$$

In this study, modified W-H models such as the uniform deformation model (UDM), uniform stress deformation model (USDM) and uniform deformation energy density model (UDEDM) are employed in evaluating the particle size and microstrain. The Williamson–Hall model is simple and effective and offers the simultaneous estimation of size and strain, however, it is limited by its assumptions of uniformity and isotropic broadening.

3.1.1.1. Uniform deformation model

The crystalline size and lattice strain of the synthesized TiO_2 and ZnO were calculated using the uniform deformation model (UDM) of the W-H analysis. The uniformity of crystal strain in all crystallographic directions is the underlying premise of the UDM. As a result, the lattice strain is regarded as an isotropic feature that is independent of the measurement direction [31]. The lattice strain-induced peak broadening can be

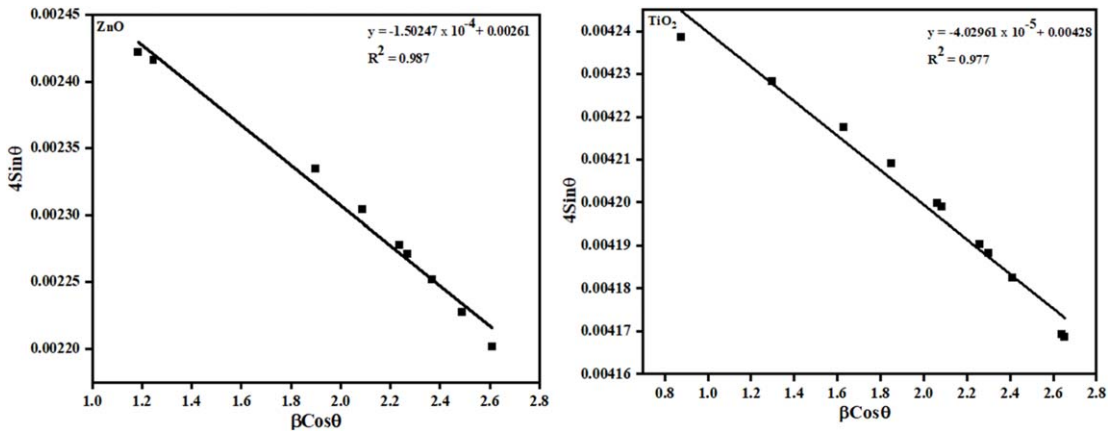

Figure 2. XRD peak profile analysis using the UDM model for ZnO and TiO_2.

expressed as:

$$\beta_{\text{strain}} = 4\varepsilon \tan\theta \tag{3}$$

For a peak with a certain hkl (β_{hkl}) value, the observed peak broadening can be interpreted as the total of the peak broadening caused by the strain and crystallite size contributions, provided that they are unrelated to one another and have a Cauchy-like profile. The observed line breadth could be expressed as equation (4) by combining equations (2) and (3):

$$\beta_{\text{hkl}} \cos\theta = \frac{K\lambda}{D} + 4\varepsilon \sin\theta \tag{4}$$

A graph of 4sinθ against β_{hkl}cosθ was generated to estimate the strain caused in the sample and crystallite. Plot strain is indicated by its slope, and crystallite size was calculated using the intercept. The W-H plot for ZnO and TiO_2 are shown in figure 2 with a linear fit that showed a good correlation of 0.977 and 0.987 respectively. For ZnO, the obtained crystallite size and lattice strain, were 55.46 nm and -1.50×10^{-4} respectively, while for TiO_2, the values are 33.82 nm and -4.03×10^{-5}. Although the atomic arrangement in nanocrystals is significantly altered by size confinement relative to their bulk equivalent, the lattice expansion or contraction in the nanocrystals is primarily responsible for the lattice strain [32]. Moreover, studies have demonstrated that lattice strain depends on shape and size [22]. The negative slope of the W-H plots indicates that the strain in the nanocrystal of TiO_2 and ZnO was the consequence of lattice contraction [33].

3.1.1.2. Uniform stress deformation model (USDM)

The assumption of homogeneity and isotropism by the UDM model is not justifiable for real crystals. To account for anisotropism in crystals, the W-H equation should be modified to include anisotropic strain. This gives rise to the uniform stress deformation model (USDM), which considers the uniformity of lattice deformation stress along all the lattice plane directions with small microstrain [34]. For a realistic crystal system, the generalized Hooke's law, which takes into account anisotropic, describes a linear relationship between stress (σ) and strain (ε), which emphasizes that it only pertains to minor strains, which arises due to size confinement in the crystal (equation (5))

$$\sigma = \varepsilon Y, \ (Y \textit{ is the Young's modulus}) \tag{5}$$

USDM took into consideration the anisotropic character of Young's modulus and stress-induced widening in the XRD peak. By inserting equation (5) into equation (4) and rearranging, we get the expression for the USDM, which takes into account the uniform stress in all crystallographic directions.

$$\beta_{\text{hkl}} \cos\theta = \frac{K\lambda}{D} + 4\sigma\frac{\sin\theta}{Y_{hkl}} \tag{6}$$

For the tetragonal TiO_2 and hexagonal ZnO crystal, Young's modulus Y_{hkl} can be expressed as equations (7) [35] and (8) [36] respectively.

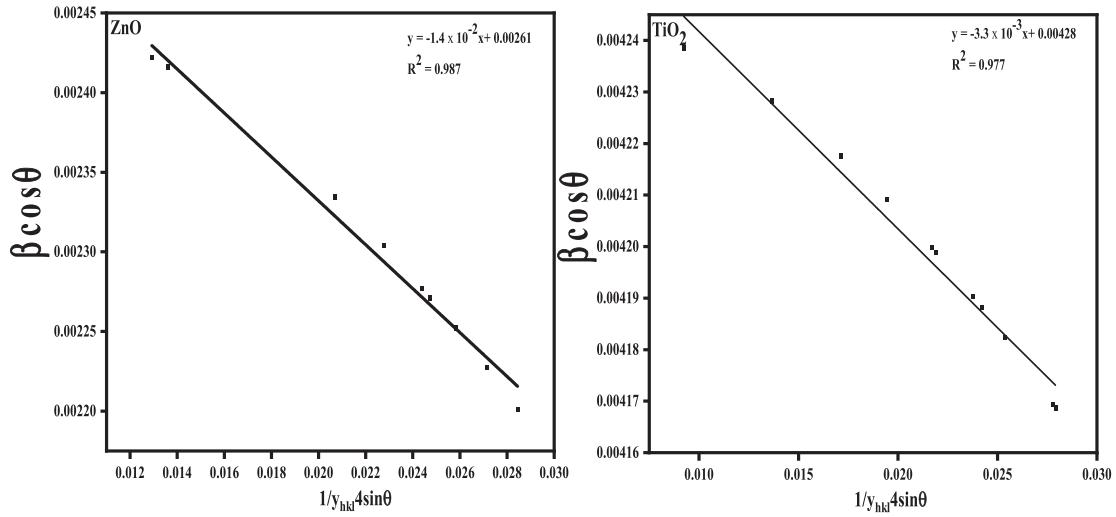

Figure 3. XRD peak profile analysis using the USDM model for ZnO and TiO_2.

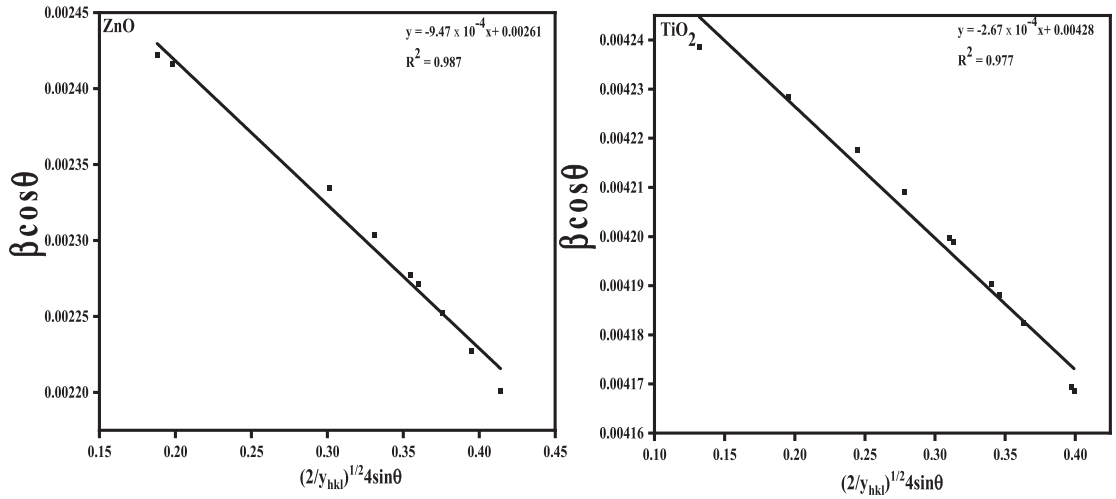

Figure 4. XRD peak profile analysis using the UDEDM model for ZnO and TiO_2.

$$E_{hkl} = \frac{\left[h^2 + \frac{(h+2k)^2}{3} + \left(\frac{a}{c}l\right)^2\right]^2}{\left[S_{11}\left(h^2 + \frac{(h+2k)^2}{3}\right)^2 + S_{33}\left(\frac{a}{c}l\right)^4 + (S_{14} + 2S_{13})\left(h^2 + \frac{(h+2k)^2}{3}\right)\left(\frac{a}{c}l\right)^2\right]} \quad (7)$$

$$E_{hkl} = \frac{[h^2 + k^2 + l^2]^2}{S_{11}(h^4 + k^4) + (2S_{12} + S_{66})h^2k^2 + (2S_{13} + S_{44})(h^2 + k^2)l^2 + S_{33}l^4} \quad (8)$$

Where S_{11}, S_{12}, S_{13}, S_{14}, S_{33}, S_{44} and S_{66} are known elastic complaints of the crystals.

Plots of $4\sigma\frac{\sin\theta}{Y_{hkl}}$ on the X-axis against $\beta_{hkl}\cos\theta$ on the Y-axis for ZnO and TiO_2 are shown in figure 3. The slope of the straight line obtained gives the stress of the crystals, while the average particle size of the crystal can be estimated from the intercept. The average particle size for TiO_2 was evaluated to be 33.82 nm, while the value for ZnO was 55.46 nm. The evaluated stress for TiO_2 and ZnO was 3.8 MPa and 13.7 MPa, respectively.

3.1.1.3. Uniform deformation energy density model (UDEDM)

Most crystals include faults caused by dislocations, defects and aggregation which suggests that the assumption of crystal isotropy and linear proportionality between stress and strain on which the UDM and USDM are based is not justified in real crystals. In addition, when the strain energy density, u is considered, the proportionality

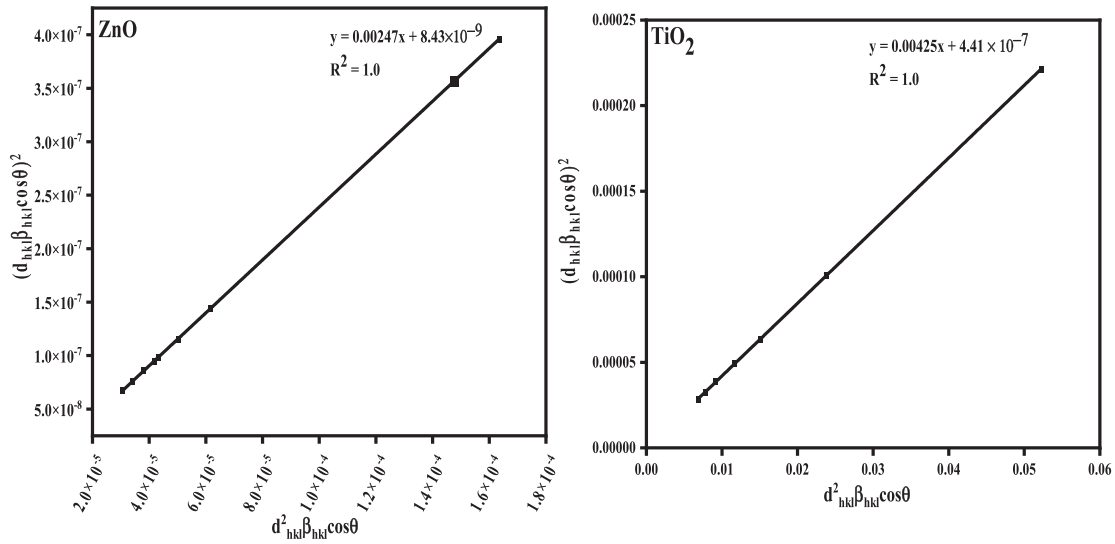

Figure 5. XRD peak profile analysis using the SSP plot for ZnO and TiO_2.

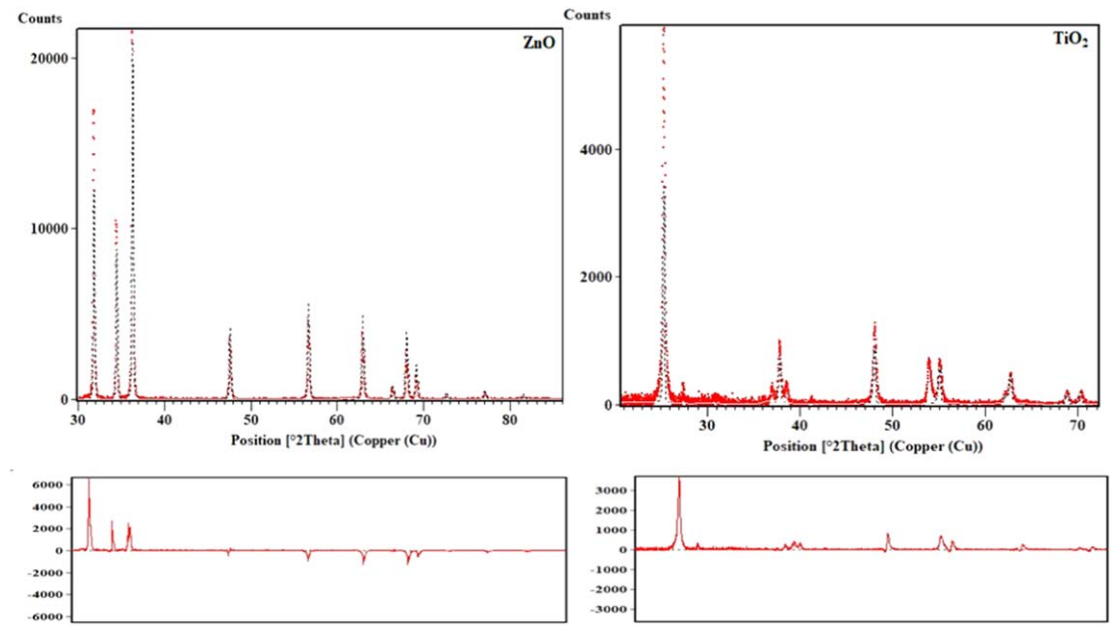

Figure 6. Rietveld analysis of ZnO and TiO_2. The red profile is the experimentally obtained diffraction, while the black profile is the calculated profile by Rietveld analysis. The bottom plot is the difference between the experimental and calculated profile.

constants associated with the stress–strain relationship become dependent [37]. The energy density for an elastic system that obeys Hooke's law can be expressed as $u = \frac{\varepsilon^2 Y_{hkl}}{2}$.

Equation (4) can then be rewritten in terms of u as (equation (9))

$$\beta_{hkl}\cos\theta = \frac{K\lambda}{D} + 4\sin\theta\left(\frac{2u}{Y_{hkl}}\right)^{\frac{1}{2}} \tag{9}$$

From figure 4, the plot between $4\sin\theta\left(\frac{2}{Y_{hkl}}\right)^{\frac{1}{2}}$ and $\beta_{hkl}\cos\theta$, the anisotropic energy density and crystallite size can be obtained from the slope and intercept, respectively. The evaluated crystallite size for TiO_2 and ZnO was 33.82 and 55.46 nm, while the anisotropic energy density was 7.12×10^{-8} KJ $m^{-3}$and 8.96×10^{-8} KJ m^{-3}

Table 1. Calculated microstructural properties from williamson–hall models, size-strain analysis and rietveld analysis.

	UDM		USDM		UDEDM		Size strain		Rietveld analysis	
Nanoparticle	Crystallite size (nm)	Strain (%)	Crystallite size (nm)	Stress (MPa)	Crystallite size (nm)	Energy density (KJ/m^3)	Crystallite size (nm)	Strain (%)	Crystallite size (nm)	Strain (%)
TiO_2	55.46	-1.5×10^{-4}	55.46	13.7	55.46	7.12×10^{-8}	58.61	1.8×10^{-4}	87.6	0.28
ZnO	33.8	-4.03×10^{-5}	33.8	3.8	33.82	8.96×10^{-8}	34.06	1.3×10^{-3}	41.9	0.003

3.1.2. Size-strain analysis

While W-H analysis considers peak broadening to be dependent on x-ray diffraction angle (2θ), the size-strain analysis considers the peak profile to be a combination of Gaussian and Forentz functions [38]. The profile broadening arising from the crystallite size is referred to as the Lorentz function, while the broadening due to strains is labelled the Gaussian function [39]. This is expressed mathematically in equation (10)

$$B_{hkl} = \beta_L + \beta_G \tag{10}$$

The equation for the SSP is given by equation (11)

$$(d_{hkl}\beta_{hkl}\cos\theta)^2 = \frac{k\lambda}{D}(\beta_{hkl}d_{hkl}^2\cos\theta) + \left(\frac{\varepsilon}{2}\right)^2 \tag{11}$$

In figure 5 plot of $(d_{hkl}\beta_{hkl}\cos\theta)^2$ on the y-axis against $\beta_{hkl}d_{hkl}^2\cos\theta$ gives a straight line with a slope equal to $\frac{k\lambda}{D}$ and intercepts equal to $\left(\frac{\varepsilon}{2}\right)^2$. The crystallite size from the SSP model for ZnO and TiO_2 was 34.06 nm and 58.61 nm, respectively and the obtained strain was 1.3×10^{-3} and 1.8×10^{-4} for TiO_2 and ZnO, respectively.

3.1.3. Rietveld analysis

Furthermore, the Rietveld analysis was used in analysing the x-ray diffraction pattern of TiO_2 and ZnO. In Rietveld analysis, diffraction patterns are constructed and then calculated about a model that is used as the crystallographic standard. The analysis simulates profile diffraction and sample structural characteristics using computed patterns [40]. The Rietveld analysis plot for ZnO and TiO_2 is shown in figure 6.

The profile of the experimental data and the calculated pattern for ZnO and TiO_2 matched perfectly, showing the presence of pure ZnO and TiO_2 nanoparticles. The difference plot shows the difference between the experimental and calculated profiles for the nanoparticles. The positive peaks show peaks in which the experimental peaks had more intensity than the calculated profile, while the negative peaks show peaks in which the experimental profile had a lower intensity compared to the calculated profile. The crystallite size and microstrain of the TiO_2 nanoparticle were evaluated to be 87.6 nm and 0.003% respectively, while the values for ZnO were 41.9 and 0.289% respectively. The Rietveld analysis offers a versatile and accurate modelling route for estimating microstructural information and refining complex structures. It is however limited to crystalline materials and also very complex.

4. Conclusion

X-ray profile broadening in crystalline materials is due mainly to crystal size and lattice strain. To estimate the crystal size and strain in green synthesized ZnO and TiO_2 nanoparticles four models: the Scherrer equation, Williamson–Hall model, size and shape plot and the Rietveld analysis were employed. The crystallite size from all the models showed good agreement as shown in the summary presented in table 1. In the Williamson–Hall a relatively constant crystallite size was obtained from the different models which shows a negligible contribution of microstrain to the profile broadening of the materials and a dominant crystallite size broadening. A significant variation in the calculated microstrain was observed among the models due to the difference in model assumption, but all the models showed the presence of only a small microstrain contribution to the profile broadening of the material. Furthermore, microstructural properties such as stress and energy density of the synthesized ZnO and TiO_2.

Acknowledgments

Dr P Mathumba, thanks to the Post-doctoral: DST-NRF Professional Development Programme for providing financial assistance. Dr MP Bilibana acknowledges the assistance received from the Department of Chemistry, North-West University.

Data availability statement

The data is available and can be shared publicly. The data that support the findings of this study are available upon reasonable request from the authors.

Author contributions

P M Data curation, formal analysis, investigation, methodology, validation, visualization, writing—original draft. M P B Conceptualization, Data curation, formal analysis, investigation, methodology, project administration, validation, visualization, writing—review and editing. O C O: Writing, analysis, and investigation. D C O: Conceptualization, data curation, formal analysis, investigation, methodology, project administration, validation, visualization, writing—original draft, writing—review and editing. All authors have read and agreed to the published version of the manuscript.

Conflicts of interest

There are no conflicts to declare.

ORCID iDs

Penny Mathumba https://orcid.org/0000-0002-2198-6978
Olalekan C Olatunde https://orcid.org/0000-0002-8245-0763
Damian C Onwudiwe https://orcid.org/0000-0002-2689-3981

References

[1] Neumann M A 2003 X-Cell: a novel indexing algorithm for routine tasks and difficult cases *J. Appl. Crystallogr.* **36** 356–65
[2] Disha S A, Sahadat Hossain M, Habib M L and Ahmed S 2024 Calculation of crystallite sizes of pure and metals doped hydroxyapatite engaging scherrer method, halder-wagner method, williamson-hall model, and size-strain plot *Results in Materials* **21** 100496
[3] Chokshi A H, Rosen A, Karch J and Gleiter H 1989 On the validity of the hall-petch relationship in nanocrystalline materials *Scr. Metall.* **23** 1679–83
[4] Schiøtz J, Vegge T, Di Tolla F and Jacobsen K W 1999 Atomic-scale simulations of the mechanical deformation of nanocrystalline metals *Phys. Rev.* B **60** 11971
[5] Hamdaoui N, Tlili D, Azizian-Kalandaragh Y, Zaidi B, Zemni S, Akl A A and Beji L 2021 Effect of Ni-doping on the structural, magnetic, and electronic properties of $La_{0.2}Sr_{0.8}MnO_3$ perovskite *J. Mater. Sci., Mater. Electron.* **32** 26984–97
[6] Kafashan H 2019 X-ray diffraction line profile analysis of undoped and Se-doped SnS thin films using Scherrer's, Williamson–Hall and size–strain plot methods *J. Electron. Mater.* **48** 1294–309
[7] Alam M K, Hossain M S, Bahadur N M and Ahmed S 2024 A comparative study in estimating of crystallite sizes of synthesized and natural hydroxyapatites using scherrer method, williamson-hall model, size-strain plot and halder-wagner method *J. Mol. Struct.* **1306** 137820
[8] Das R, Nath S S and Bhattacharjee R 2010 Preparation of linoleic acid capped gold nanoparticles and their spectra *Physica* E **43** 224–7
[9] Santos C I D L, Carvalho M S, Raphael E, Dantas C, Ferrari J L and Schiavon M A 2016 Synthesis, optical characterization, and size distribution determination by curve resolution methods of water-soluble CdSe quantum dots *Mater. Res.* **19** 1407–16
[10] Akl A A and Hassanien A S 2021 Comparative microstructural studies using different methods: effect of Cd-addition on crystallography, microstructural properties, and crystal imperfections of annealed nano-structural thin $Cd_xZn_{1-x}Se$ films *Physica* B **620** 413267
[11] Zak A K, Majid W A, Abrishami M E and Yousefi R 2011 X-ray analysis of ZnO nanoparticles by williamson–hall and size–strain plot methods *Solid State Sci.* **13** 251–6
[12] Al-Hazmi G H, El-Desouky M G and El-Bindary A A 2022 Synthesis, characterization and microstructural evaluation of ZnO nanoparticles by william-hall and size-strain plot methods *Bull. Chem. Soc. Ethiop.* **36** 815–29
[13] Vanaraj S, Keerthana B B and Preethi K 2017 Biosynthesis, characterization of silver nanoparticles using quercetin from clitoria ternatea l to enhance toxicity against bacterial biofilm *J. Inorg. Organomet. Polym. Mater.* **27** 1412–22
[14] Biswas A, Vanlalveni C, Adhikari P P, Lalfakzuala R and Rokhum L 2018 Green biosynthesis, characterisation and antimicrobial activities of silver nanoparticles using fruit extract of solanum viarum *IET Nanobiotechnol.* **12** 933–8
[15] Vanlalveni C, Lallianrawna S, Biswas A, Selvaraj M, Changmai B and Rokhum S L 2021 Green synthesis of silver nanoparticles using plant extracts and their antimicrobial activities: a review of recent literature *RSC Adv.* **11** 2804–37
[16] Naiel B, Fawzy M, Halmy M W A and Mahmoud A E D 2022 Green synthesis of zinc oxide nanoparticles using sea lavender (Limonium pruinosum L. Chaz.) extract: characterization, evaluation of anti-skin cancer, antimicrobial and antioxidant potentials *Sci Rep.* **12** 20370
[17] Doan Thi T, Nguyen T, Thi Y, Ta Thi K, Phan B and Pham K 2020 Green synthesis of ZnO nanoparticles using orange fruit peel extract for antibacterial activities *RSC Adv.* **10** 23899–907
[18] Thakur B K, Kumar A and Kumar D 2019 Green synthesis of titanium dioxide nanoparticles using azadirachta indica leaf extract and evaluation of their antibacterial activity *S. Afr. J. Bot.* **124** 223–7
[19] Nasrollahzadeh M and Sajadi S M 2015 Synthesis and characterization of titanium dioxide nanoparticles using euphorbia heteradena jaub root extract and evaluation of their stability *Ceram. Int.* **41** 14435–9
[20] Sivaranjani V and Philominathan P 2016 Synthesize of titanium dioxide nanoparticles using moringa oleifera leaves and evaluation of wound healing activity *Wound Medicine* **12** 1–5
[21] Mudau H S, Mokoboki H K, Ravhuhali K E and Mkhize Z 2022 Effect of soil type: qualitative and quantitative analysis of phytochemicals in some browse species leaves found in savannah biome of south africa *Molecules* **27** 1462
[22] Olatunde O C, Marzouki R, Brahmia A and Onwudiwe D C 2023 Lattice strain analysis of antimony sulphide nanorods *J. Cluster Sci.* **34** 2017–27

[23] Saha C, Ghosh S K, Kumari P, Perla V K, Singh H and Mallick K 2024 Enhanced catalytic performance of carbon nitride-functionalized titanium dioxide through efficient oxygen vacancy defect engineering for electrochemical recognition of epinephrine *Electrocatalysis* **15** 173–182
[24] Kardeş M and Öztürk K 2023 A comparative investigation of photocatalyst ZnO nanorods grown on different seed layers: influence of annealing temperature and atmosphere *Res. Chem. Intermed.* **50** 353–372
[25] Yadeta Gemachu L and Lealem A 2024 Birhanu, green synthesis of ZnO, CuO and NiO nanoparticles using neem leaf extract and comparing their photocatalytic activity under solar irradiation *Green Chem. Lett. Rev.* **17** 2293841
[26] Zhang L, Jiang Y, Ding Y, Daskalakis N, Jeuken L, Povey M, O'Neill A J and York D W 2010 Mechanistic investigation into antibacterial behaviour of suspensions of ZnO nanoparticles against *E. coli J. Nanopart. Res.* **12** 1625–36
[27] Baek M, Kim M K, Cho H J, Lee J A, Yu J, Chung H E and Choi S J 2011 Factors influencing the cytotoxicity of zinc oxide nanoparticles: particle size and surface charge *J. Phys. Conf. Ser.* **304** 012044
[28] Naseer M, Aslam U, Khalid B and Chen B 2020 Green route to synthesize zinc oxide nanoparticles using leaf extracts of cassia fistula and melia azadarach and their antibacterial potential *Sci Rep.* **10** 9055
[29] Aravind M, Amalanathan M and Mary M S M 2021 Synthesis of TiO_2 nanoparticles by chemical and green synthesis methods and their multifaceted properties *SN Appl. Sci.* **3** 409
[30] Das R and Sarkar S 2015 Determination of intrinsic strain in poly (vinylpyrrolidone)-capped silver nano-hexapod using x-ray diffraction technique *Curr. Sci.* **109** 775–8
[31] Mote V, Purushotham Y and Dole B 2012 Williamson-hall analysis in estimation of lattice strain in nanometer-sized ZnO particles *Journal of Theoretical and Applied Physics* **6** 1–8
[32] Nath D, Singh F and Das R 2020 X-ray diffraction analysis by williamson-hall, halder-wagner and size-strain plot methods of CdSe nanoparticles-a comparative study *Mater. Chem. Phys.* **239** 122021
[33] Sarkar S and Das R 2018 Shape effect on the elastic properties of Ag nanocrystals *Micro & Nano Letters* **13** 312–5
[34] Sarkar S and Das R 2018 Determination of structural elements of synthesized silver nano-hexagon from x-ray diffraction analysis *Indian J. Pure Appl. Phys.* **56** 765–72
[35] Zhang J M, Zhang Y, Xu K W and Ji V 2007 Anisotropic elasticity in hexagonal crystals *Thin Solid Films* **515** 7020–4
[36] Zhang J-M, Zhang Y, Xu K-W and Ji V 2008 Young's modulus surface and poisson's ratio curve for tetragonal crystals *Chin. Phys.* B **17** 1565
[37] Devesa S, Rooney A P, Graça M P, Cooper D and Costa L C 2021 Williamson-hall analysis in estimation of crystallite size and lattice strain in $Bi_{1.34}Fe_{0.66}Nb_{1.34}O_{6.35}$ prepared by the sol-gel method *Mater. Sci. Eng.* B **263** 114830
[38] Dey P C and Das R 2021 Impact of silver doping on the crystalline size and intrinsic strain of MPA-capped CdTe nanocrystals: a study by williamson–hall method and size–strain plot method *J. Mater. Eng. Perform.* **30** 652–60
[39] Khorsand Zak A, Majid W H A, Abrishami M E and Yousefi R 2011 X-ray analysis of ZnO nanoparticles by Williamson–Hall and size–strain plot methods *Solid State Sci.* **13** 251–6
[40] Oliveira Y L, Costa M J S, Jucá A C S, Silva L K R, Longo E, Arul N S and Cavalcante L S 2020 Structural characterization, morphology, optical and colorimetric properties of NiWO4 crystals synthesized by the co-precipitation and polymeric precursor methods *J. Mol. Struct.* **1221** 128774